Proceedings of the Seventh International Conference on
Railway Technology: Research, Development and Maintenance
Edited by: J. Pombo
Civil-Comp Conferences, Volume 15, Paper 6.7
Civil-Comp Press, Edinburgh, United Kingdom, 2026
ISSN: 2753-3239, doi: 10.4203/ccc.15.6.7

Influence of Eccentric Wheel–Rail Impact Loading on Rail Stress in Fixed Railway Crossings

H. Vilhelmson, B. A. Pålsson, J. C. O. Nielsen and J. Brouzoulis

Department of Mechanical Engineering/CHARMEC, Chalmers University of Technology, Gothenburg, Sweden

Abstract

The effect of eccentric loading on the structural response of the crossing rail that occurs when a vehicle passes in the trailing direction (move) through a crossing panel, i.e. when the wheel transitions from the crossing nose to the wing rail, is studied utilising two models that employ different representations of the crossing rail. One model is based on beam finite elements with step-wise varying properties to capture the variation in geometry, while the other uses 3D solid elements representing the complete rail geometry. The results show that the stress state is predominantly uniaxial. While the Euler-Bernoulli bending stress provides an accurate description of the bending stress caused by the impact in the facing move, it significantly underestimates the bending stress that occurs in the trailing move due to the eccentric position of the impact load on the wing rail. By including the contribution due to Vlasov torsion in the bending stress evaluation, the bending stress in the crossing rail can be accurately represented for both facing and trailing moves using beam elements.

Keywords: railway, switches & crossings, turnout, 3D finite element model, multibody simulation, dynamic vehicle–track interaction, Vlasov torsion, bending stress

1 Introduction

Railway turnouts, often referred to as Switches & Crossings (S&Cs), enable trains to traverse intersecting tracks. During the wheel transfer from the wing rail to the crossing nose (or vice-versa), the conicity of the wheel in combination with the variation in rail geometry along the crossing results in a wheel–rail excitation that is characterised by a dip in the vertical wheel trajectory. This induces wheel–rail impact loading and leads to subsequent damage to the running surfaces of wheels and rails (plastic deformation, rolling contact fatigue and wear), noise and vibration, and differential settlement of the supporting foundation. Depending on the location of the impact, significant torsion of the crossing rail (the monoblock casting that contains both the wing rail and the crossing nose) may occur. It can also lead to bending-induced rail fatigue and sleeper cracking if the crossing is not properly maintained.

Damage to the running surface is a major contributor to the fact that the maintenance costs for turnouts is significantly higher than for plain track. The cost of maintenance of an S&C unit has been estimated to be equivalent to that of about 0.3 km of plain line track [1]. The high maintenance demand provides a strong incentive to optimise the S&C to reduce the deterioration-driving mechanisms described above. Such optimisation efforts generally focus on the critical regions of the S&C where wheel transfer between rails occur, such as the switch panel or the crossing panel (see Figure 1), the latter being the subject of this paper. Examples of previous optimisation studies specifically addressing the crossing panel include [2–11].

The most common strategy for reducing deterioration in the crossing panel is to mitigate the dynamic impact load caused by the wheel transfer, typically analysed using multibody simulation or FEM. This is a problem characterised by complex dynamic vehicle–track interaction, and, consequently computational efficiency becomes central to the feasibility of optimisation procedures aiming to reduce the deterioration of the crossing panel. A widely adopted method for reducing the dynamic impact loads is to introduce softer rail pads or under-sleeper pads (USP), although this can result in increased rail stress. This emphasises the importance of accurate stress estimation within the numerical models used in such optimisation studies.

In the majority of previous optimisation studies, the rails are modelled using beam elements with step-wise varying element properties, or the track is even further simplified using moving mass-spring systems. Although some fully three-dimensional FEM models have been developed, their computational effort generally renders them unsuitable for optimisation studies involving dynamic vehicle–track interaction, for example [12–14]. Generally, the dynamics of the wheel passage can be captured adequately using multibody simulation models, while the primary advantage of full 3D FEM models lies in their ability to resolve the detailed stress field in 3D.

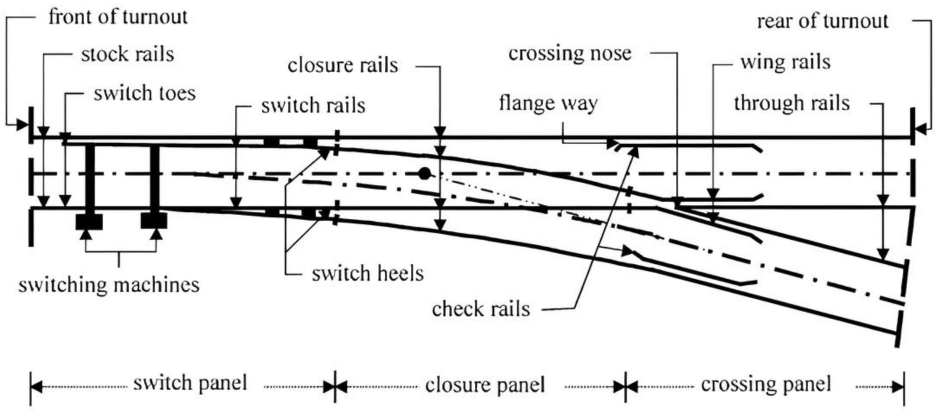

Figure 1: Schematic illustration of a turnout (S&C) and its components.

Although the maximum stress is sometimes assessed using simplified metrics such as maximum displacement [5, 6], the multibody simulation models that calculate rail foot stresses generally do so using Euler–Bernoulli beam theory [4,15]. This approach assumes that the relevant stresses occur only due to one-dimensional bending of the rail, thereby neglecting any potential effects of eccentric loading. Such eccentric loading occurs consistently in the trailing move when the wheel impact lands on the wing rail and can have a significant effect on the loading of the crossing rail [16]. Despite this, its effects have not been studied in the literature. In this paper, the increase in crossing rail bending stress arising from Vlasov torsion is evaluated, and a new stress-evaluation method that incorporates the contribution from Vlasov torsion is proposed.

2 Simulation models

As discussed above, numerically modelling the dynamic vehicle–track interaction occurring at a crossing requires substantial computational effort. Consequently, most models rely on multibody simulation tools, which limits direct access to structural quantities such as rail stress. In this study, two modelling approaches are compared: (1) FEM models are used to examine the rail stress under a highly simplified static load case, using both beam and 3D solid elements, while (2) a multibody-based approach using beam elements is used to assess how rail stress can be evaluated when the dynamic vehicle–track interaction in the crossing panel is considered, subject to the simplifications inherent in that modelling framework. The two models are briefly described in the following sections.

2.1 Multibody simulation model

The applied simulation model of the crossing panel used in this work is a representation of the 60E1-500-1:12 demonstrator turnout installed in the Austrian network as a part of the In2Track projects within the EU-funded Shift2Rail research programme [17]. The structural finite element model of the crossing panel, comprising 37 sleeper spans and originally developed, calibrated, and validated in [15], has been implemented in the commercial MBS software Simpack.

The model consists of two layers of bushing elements, one representing the sleeper support (a combination of the under-sleeper pad and the ballast/subgrade) and one for the rail fastening. For the rail fastening system, the nominal values for stiffness and damping are taken from the Shift2Rail demonstrator turnout studied in [15, 18]. For the ballast, the calibrated ballast stiffness from [15, 18] is used. The stiffness and damping parameters for the track are given in Table 1. Rails and sleepers are modelled as substructures of beam elements. These substructures are generated using Craig-Bampton model reduction [19] applied to individual finite element beam models of the crossing rail, stock rails and sleepers, respectively. The model incorporates scanned crossing rail geometries obtained from in-situ crossings and scanned wheel profiles from in-service wheels. In addition, the cross-sectional properties used for the beam elements, such as the area moment of inertia, vary along the crossing rail and have been derived from a CAD model.

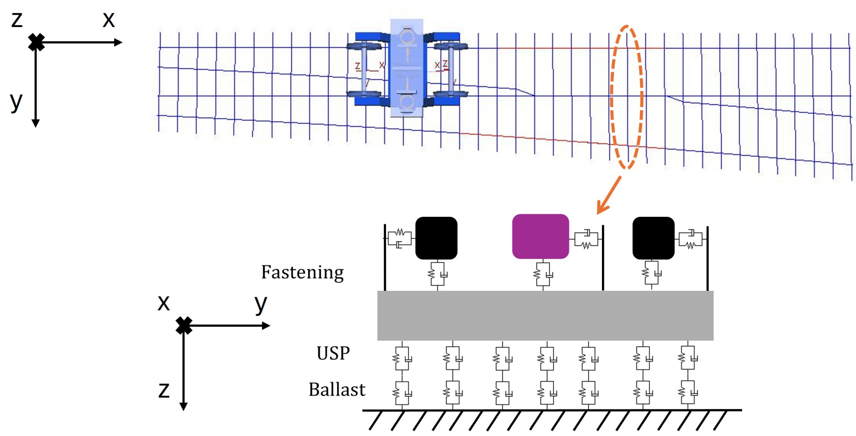

Figure 2: Full multibody simulation model and detailed setup for one sleeper.

Table 1: Stiffness and damping parameters for the track.

Ballast bed modulus	120 MN/m^3
Combined (support) ballast bed and USP damping modulus	167 kNs/m^3
Rail fastening stiffness	25-50 MN/m
Rail fastening viscous damping	5-10 kNs/m

2.2 Finite element model

In parallel, a finite element model of the crossing panel has been generated in which the stock rails and sleepers are represented using beam elements, while the crossing rail is modelled either with 3D solid elements, see Figure 3, or with beam elements, enabling direct comparison between the two modelling approaches. For the bushing elements representing the rail fastenings and sleeper support, the same stiffness and damping values are applied as in the multibody simulation model. In the beam element representation of the crossing rail, the cross-sectional properties, such as the area moment of inertia, vary along its length and have been determined from the corresponding 3D CAD model. The number of beam elements per rail per sleeper bay is 32.

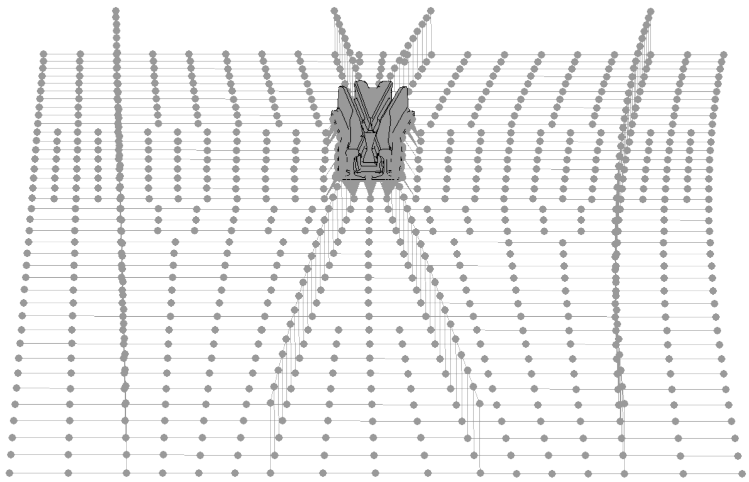

Figure 3: Finite element model of the crossing panel, including a 3D model of the crossing rail.

3 Vlasov torsion contribution

Although the geometry of crossing rails used in railway networks varies across countries and infrastructure managers, the design of the internal cross-sectional geometry (running surface excluded) is generally based on the same principles. Typically, the crossing rail design is varied between two internal geometries, one which is used above each sleeper, and one which is used between the sleepers, with a relatively abrupt transition between the two. Generally, the geometry used above the sleepers contains more material than the geometry between the sleepers. Two examples from a field scanned crossing rail are shown in Figures 4a and 4b. As mentioned, the precise shapes of these two geometries may differ significantly between manufacturers, although the underlying design philosophy remains consistent. The location of the maximum crossing rail stress is generally seen for the cross-section situated between the sleepers, near the interface between the two cross-sections, where stress concentrations commonly arise due to the abrupt change in shape.

Between the sleepers, the crossing rail typically features an open cross-section, such as the one presented in Figure 4a. Cross-sections of this type are known to be susceptible to Vlasov torsion, which introduces an additional contribution to the bending stress when the rail is subjected to a torsional load. By contrast, the closed cross-section used above sleepers is generally less prone to Vlasov torsion.

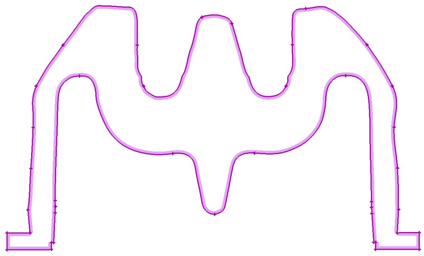

(a) A typical crossing rail cross-section used between sleepers.

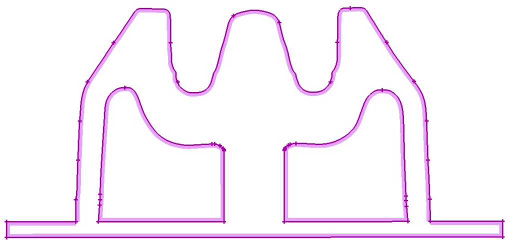

(b) A typical crossing rail cross-section used above sleepers.

Figure 4: Side-by-side cross-sections for the crossing rail.

In this paper, the beam element model presented in [15] is extended to also include the torsional degree of freedom. To study the effect of the eccentric loading that occurs in the trailing move on the bending stress in the rail foot, the Vlasov term is added to the original Euler–Bernoulli bending stress expression, see Equation 1,

$$\sigma_{xx}(x, y, z) = -\frac{M(x)}{I(x)} z(x) + \frac{B(x)}{K_w(x)} \Psi(x, y, z) \tag{1}$$

where $\Psi(x, y, z)$ is the warping function along the beam, which is here simplified to a single representative value for each cross-section, namely its maximum. Furthermore, $B(x)$ is the bi-moment, and $K_w(x)$ is the warping constant which is dependent on the cross-sectional geometry. The torsional and warping properties of each cross-section are determined from a 3D CAD model of the crossing rail. The bi-moment along the crossing rail is defined as

$$B(x) = -EK_w(x) \frac{d^2\phi(x)}{dx^2} \tag{2}$$

where $\phi(x)$ is the torsion of the crossing rail.

4 Effect of eccentric loading

To enable a clear comparison between the two running directions, it is assumed that the wheel–rail contact force and the longitudinal position of the impact are the same for both the trailing and facing moves. Two load cases are considered. For the 3D model, a vertical static load is applied at a fixed position either on the crossing nose (facing move) or on the wing rail (trailing move). For the beam model, the trailing move load case consists of a vertical static load combined with a torsional moment, calculated based on the lateral offset to the application point of the trailing move load in the 3D model, see Figure 5. For the facing move load case, only the static load is applied. In Section 5, the MBS model will in be used to account for potential variations in impact load position and load due to the dynamics of the wheel transition.

First, the 3D version of the crossing rail is studied for both running directions. The stress state is evaluated along all lateral coordinates on the bottom of the crossing rail, partitioned into 1 cm wide slices along the longitudinal axis. For each slice, the maximum stress is extracted and plotted in Figure 6. The most notable result is the increase in bending stress (normal stress in the longitudinal direction) due to the eccentric loading, as the maximum bending stress can be seen to be significantly higher for the trailing move. For the trailing move load case, periodic peaks in bending stress appear along the crossing rail, located adjacent to each reinforced cross-section. These peaks arise due to the Vlasov contribution to the bending stress presented in Equation 1. At each reinforced cross-section, the abrupt increase in torsional stiffness of the crossing rail produces an increase in the bi-moment, as defined in Equation 2, which in turn causes the observed stress peaks.

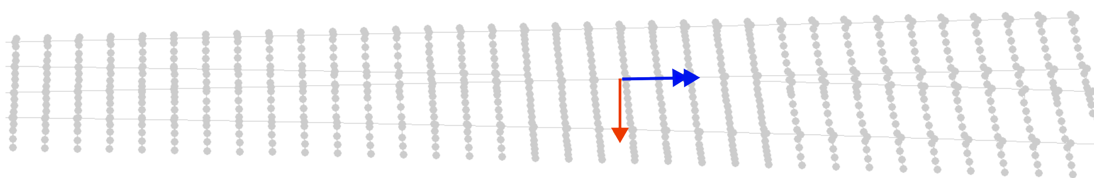

Figure 5: Finite element model of the crossing panel, including a beam representation of the crossing rail. The applied vertical static force is depicted in red, and the torsional moment in blue.

As previously mentioned, earlier studies have used Euler–Bernoulli beam theory to evaluate bending stresses in crossing rails. To verify that the stress state in the crossing rail is indeed uniaxial, i.e. that bending stress alone is an acceptable metric to determine the stress state, the principal stresses and the bending stress for the trailing move are compared in Figure 7. The results show that the stress state near the maximum bending stress is very close to uniaxial, indicating that the shear stresses arising from the eccentric loading position are small.

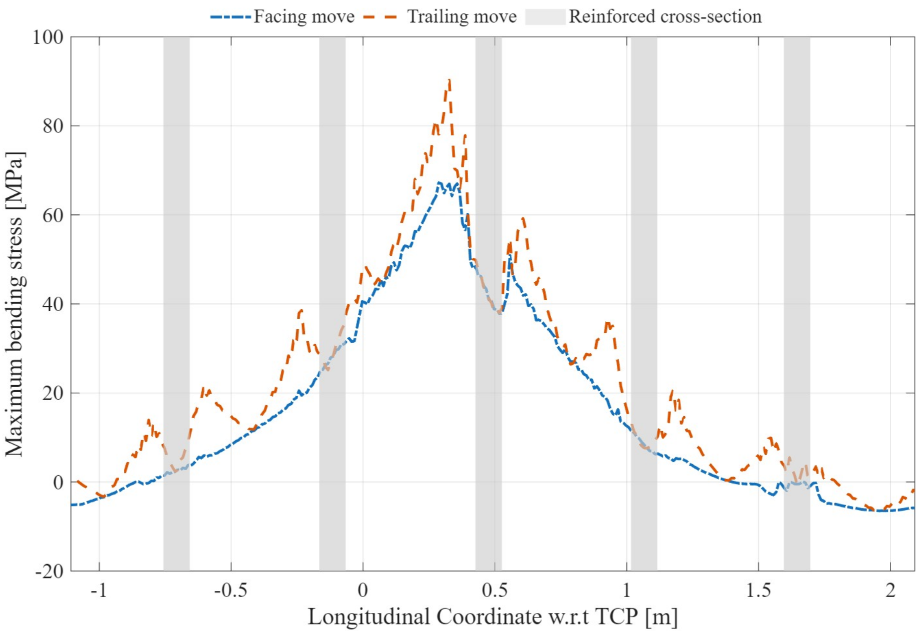

Figure 6: Maximum bending stress obtained from the 3D model along the longitudinal coordinate of the crossing rail, measured with respect to the theoretical crossing point (TCP), for both facing and trailing move load cases.

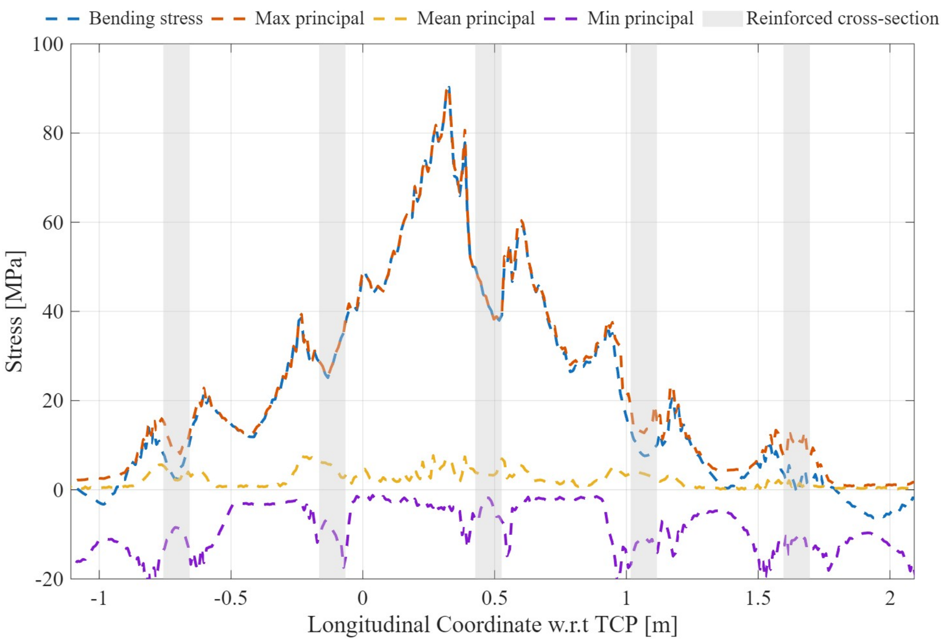

Figure 7: Maximum bending stress and maximum of each principal stress (minimum of the minimum principal stress) along the longitudinal coordinate of the crossing rail, measured with respect to the theoretical crossing point (TCP), for the trailing move load case.

Now the same static load cases are studied using the beam version of the model, with an applied moment in addition to the static force, to replicate the eccentric loading present in the trailing move. The Euler–Bernoulli bending stress is calculated, both with and without the Vlasov contribution (the bending stress including the Vlasov contribution is here referred to as the Euler–Bernoulli–Vlasov bending stress). These two beam-model stress measures are compared with the stress obtained from the 3D model in Figures 8 and 9, showing the facing and trailing move load cases, respectively. The Euler–Bernoulli bending stress yields identical values for the facing and trailing moves, and the significant increase in bending stress observed for the trailing move in the 3D model, see Figure 6, is entirely absent. Thus, the Vlasov contribution in the facing move is negligible. However, this applies specifically at the impact position, where the eccentric loading is negligible for the facing move. As the wheel progresses further along the wing rail, an increased contribution from torsion can be expected. In the trailing move, the increase in maximum bending stress is pronounced, resulting in an increase of the maximum bending stress by 36%. The same periodic pattern that was identified in the 3D model for the trailing move appears only when the Vlasov contribution is included. With the added Vlasov contribution, the correlation between the beam and 3D models has improves substantially for the trailing move load case, see Figure 9.

When Vlasov torsion is accounted for, the discrepancy between the 3D and beam models becomes consistent across both load cases, with ratios of 1.27 and 1.29 for the trailing and facing moves, respectively. The remaining discrepancy is attributed to local stress concentrations arising from the complex bottom geometry of the crossing rail.

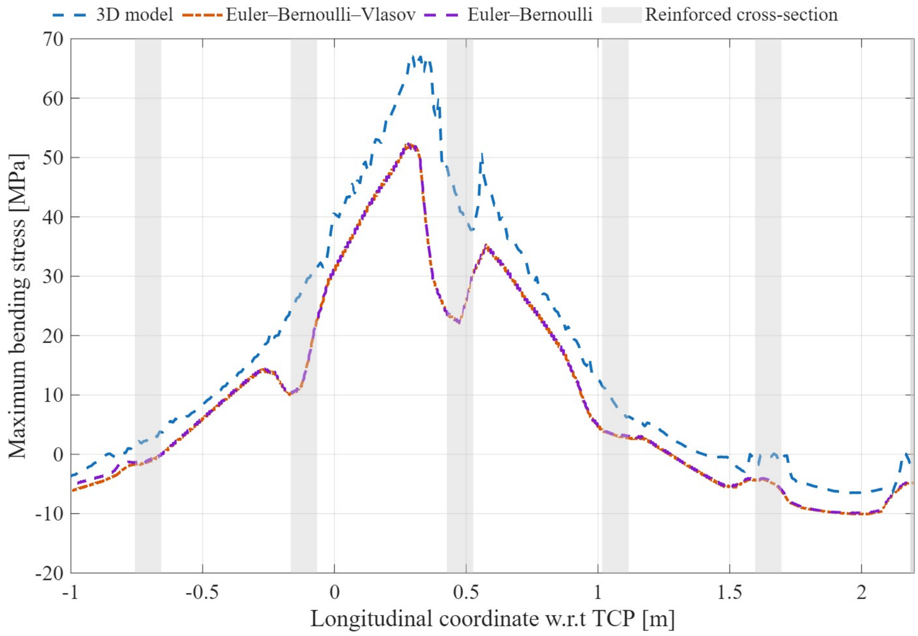

Figure 8: Bending stress with and without the Vlasov torsion contribution using the beam model, compared to the 3D model. Both models are subjected to the facing move load case.

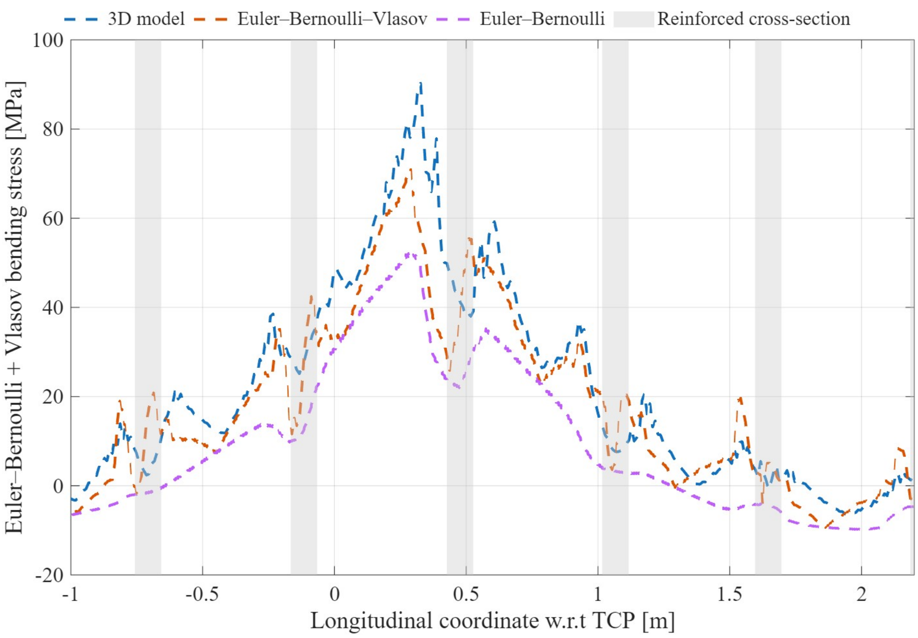

Figure 9: Bending stress with and without the Vlasov torsion contribution using the beam model, compared to the 3D model. Both models are subjected to the trailing move load case.

5 Validation against measurement data

In the preceding results, it has been demonstrated that the direction of travel can have a significant effect on the crossing rail stress for a static load case. To examine the effect of the running direction while also accounting for the dynamics of the crossing transition, the MBS model has been used. In [15], this model was validated (for facing move traffic) against an extensive set of measurement data from the demonstrator S&C, including displacements and stresses in both sleepers and the crossing rail, as well as sleeper–ballast contact pressures.

The bending stress with the added Vlasov term is validated against the measurement data for both the facing and trailing moves in Figure 10, where the measurement positions are located on the rail foot. A substantial improvement is seen for the trailing move, in which torsional loading is greatest due to the eccentric impact loading, but some improvement is also seen for the facing move. For the facing move, the first peak is significantly lower than the second one, a behaviour that was consistently observed across all bogie passages.

However, a non-negligible discrepancy between the simulated and measured stresses remains for all but one of the peaks. This residual discrepancy is attributed to local stress concentrations associated with the complex bottom geometry of the crossing rail, resulting in stress-raising effects at the measurement location. Incorporating a suitable stress-raising factor would likely yield a more accurate stress prediction and further improve the agreement with the measurement data. However, this refinement lies outside the scope of the present study.

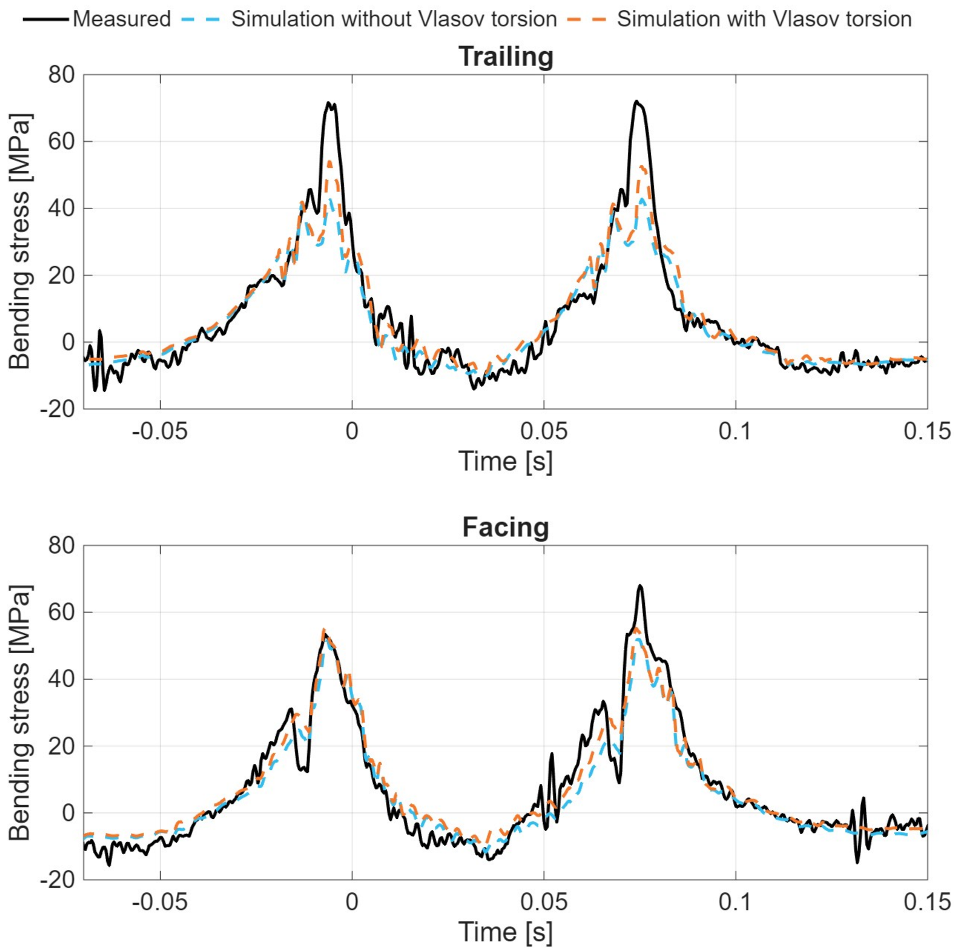

Figure 10: Simulated bending stress, with and without the Vlasov torsion contribution, obtained from the MBS model compared with the measurement data.

6 Conclusion

The effect on rail stress due to eccentric impact loading has been studied using two models that employ different representations of the crossing rail. The stress state in the crossing rail is predominantly uniaxial for a load case that includes the torsion caused by an eccentric loading. However, while the Euler–Bernoulli bending stress provides an accurate representation of the bending stress for facing move traffic, it significantly underestimates the bending stress that occurs in the trailing move. It has been shown that the increase in bending stress associated with the eccentric loading position is caused by Vlasov torsion. When the Vlasov contribution to the bending stress is included, the discrepancies between the beam and 3D models become consistent for both running directions. The remaining discrepancy factor is attributed to stress concentrations caused by the complex bottom geometry of the crossing rail. In conclusion, when employing a beam-element formulation in the simulation model, Vlasov torsion must be considered in any structural optimisation of the crossing panel to ensure an accurate assessment of the rail stress.

Acknowledgements

The current work is part of the activities within the Centre of Excellence CHARMEC (CHAlmers Railway MEChanics, www.chalmers.se/charmec). Parts of the study have been funded within the European Union's Horizon 2020 research and innovation programme in the Europe's Rail project R2DATO under grant agreement no. 101102001 and IAM4RAIL under grant agreement no. 101101966. The computations were enabled by resources provided by the National Academic Infrastructure for Supercomputing in Sweden (NAISS), and the Swedish National Infrastructure for Computing (SNIC) at C3SE, partially funded by the Swedish Research Council through grant agreement no. 2022-06725.

References

[1] Capacity4Rail. Deliverable D1.3.1, Operational failure modes of switches and crossings, 2015. 61 pp.

[2] Pålsson BA. Optimisation of railway crossing geometry considering a representative set of wheel profiles. *Vehicle System Dynamics*, 53(2):274–301, 2015.

[3] Nicklisch D, Kassa E, Nielsen JCO, et al. Geometry and stiffness optimization for switches and crossings, and simulation of material degradation. *Proceedings of the Institution of Mechanical Engineers, Part F: Journal of Rail and Rapid Transit*, 224(4):279–292, 2010.

[4] Grossoni I, Bezin Y, and Neves S. Optimisation of support stiffness at railway crossings. *Vehicle System Dynamics*, 56:1–25, 2017.

[5] Lau A. Numerical simulation of switch and crossing towards an optimized turnout design. PhD thesis, Norwegian University of Science and Technology, Trondheim, Norway, 2018.

[6] Wan C, Markine VL, and Shevtsov I. Optimisation of the elastic track properties of turnout crossings. *Proceedings of the Institution of Mechanical Engineers, Part F: Journal of Rail and Rapid Transit*, 230(2):360–373, 2016.

[7] Markine VL and Wan C. Performance optimised geometry of railway crossings: Design and implementation. *International Journal of Railway Technology*, 5:1–25, 2016.

[8] In2Track. D2.2 Enhanced S&C whole system analysis, design and virtual validation, 2020. 411 pp.

[9] In2Track2. D01.2 Research into enhanced track and switch and crossing system 2, 2021. 122 pp.

[10] Skrypnyk R, Ekh M, Nielsen JCO, et al. Prediction of plastic deformation and wear in railway crossings – Comparing the performance of two rail steel grades. *Wear*, 428-429:302–314, 2019.

[11] Li X, Nielsen JCO, and Torstensson PT. Simulation of wheel–rail impact load and sleeper–ballast contact pressure in railway crossings using a Green's function approach. *Journal of Sound and Vibration*, 463:114949, 2019.

[12] Ma Y, Mashal AA, and Markine VL. Modelling and experimental validation of dynamic impact in 1:9 railway crossing panel. *Tribology International*, 118:208–226, 2018.

[13] S Gapp. *Holistic Damage Assessment of Switches and Crossings*. PhD thesis, Technical University of Leoben, Austria, 2025.

[14] Otorabad HA, Bezin Y, Grossoni I, et al. Finite element analysis of a crossing panel under dynamic moving load – Effect of support conditions and implications on foot fatigue. *Proceedings of the Institution of Mechanical Engineers, Part F: Journal of Rail and Rapid Transit*, 237(5):563–575, 2023.

[15] Pålsson BA, Vilhelmson H, Nielsen JCO, et al. Dynamic vehicle–track interaction and loading in a railway crossing panel – Calibration of a structural track model to comprehensive field measurements. *Vehicle System Dynamics*, 62(11):2810–2836, 2024.

[16] Nijman E, Buchegger B, Pickl W, et al. The influence of the lateral contact point trajectory and the rotation of the monoblock on the impact loads in railway turnouts. *Journal of Sound and Vibration*, 536:117118, 2022.

[17] In2Track. Deliverable D1.1, Enhanced S&C whole system analysis, design and virtual validation (midterm report), 2021.

[18] Vilhelmson H, Pålsson BA, Nielsen JCO, et al. Dynamic vehicle–track interaction and structural loading in a crossing panel – Calibration and assessment of a model with a 3D representation of the crossing rail. *Vehicle System Dynamics*, 62(12):3168–3190, 2024.

[19] Craig RR and Bampton MCC. Coupling of substructures for dynamic analyses. *AIAA Journal*, 6(7):1313–1319, 1968.